Large energy storage density, low energy loss and highly stable (Pb0.97La0.02)(Zr0.66Sn0.23Ti0.11)O3 antiferroelectric thin-film capacitors

Zhengjie Lin, Ying Chen, Zhen Liu, Genshui Wang, Denis Remiens, Xianlin Dong

Journal of the European Ceramic Society 38 (2018) 3177–3181

Large energy storage density, low energyloss and highly stable$(Pb_{0.97}La_{0.02}(Zr_{0.66}Sn_{0.23}Ti_{0.11})O_3$ antiferroelectric thin-film capacitors

Zhengjie Lin[a,b], Ying Chen[a,*], Zhen Liu[a], Genshui Wang[a], Denis Rémiens[c], Xianlin Dong[a,*]

[a] Key Laboratory of Inorganic Functional Materials and Devices, Shanghai Institute of Ceramics, Chinese Academy of Sciences, 1295 Dingxi Road, Shanghai 200050, People's Republic of China

[b] University of Chinese Academy of Sciences, No. 19(A) Yuquan Road, Shijingshan District, Beijing 100049, People's Republic of China

[c] Institute of Electronics, Microelectronics and Nanotechnology (IEMN)-DOAE, UMR CNRS 8520, Université des Sciences et Technologies de Lille, 59652 Villeneuve d'Ascq Cedex, France

Article Info

Keywords:
Energy storage
Antiferroelectric
Thin-film
PLZST

ABSTRAC T

In this work, high performance $(Pb_{0.97}La_{0.02})(Zr_{0.66}Sn_{0.23}Ti_{0.11})O_3$ polycrystalline antiferroelectric thin-film was successfully fabricated on $(La_{0.7}Sr_{0.3})MnO_3/Al_2O_3(0001)$ substrate via a cost-effectively chemical solution method. A large recoverable energy storage density (W_{re}) of 46.3 J/cm^3 and high efficiency (η) of 84% were realized simultaneously under an electric field of 4 MV/cm by taking full advantage of the linear dielectric response after the electric field induced antiferroelectric-ferroelectric transition. Moreover, the PLZST thin-film displayed high temperature stability. With increasing temperature from 300 K to 380 K, the W_{re} decreased only 1.3%. The film also exhibited good fatigue endurance up to 1×10^5 cycling under an electric field of 2.2 MV/cm. Our work underlines the importance of the interface quality between the film and the substrate and the important role of linear dielectric answer after saturation in the improvement of the energy storage density and efficiency of antiferroelectric materials.

1. Introduction

In recent years, the demand for dielectric capacitors with low loss, high energy-storage density, high stability and fast discharge speed is increasing for power electronic devices due to the rapid development of electronic industry [1–3]. A high energy loss causes not only a waste of energy but also a heating problem which will lead to a performance deterioration of the electronics. For energy storage, it is well known that antiferroelectric (AFE) is a very good candidate in comparison to linear dielectric (LD) and ferroelectric (FE) materials. AFE materials possess higher energy storage density due to their high saturated polarization and small remnant polarization [4–7]. However, the efficiency of typical AFE materials is quite low, which is limited by a large difference $^{\triangle}E$ between E_{FA} and E_{AF} with $\triangle E = E_{AF} - E_{FA}$, where E_{AF} and E_{FA} are the forward and backward threshold fields, respectively. So it is of practical significance to fabricate AFE materials with both high W_{re} and η. But this is still a problem hanging on. For example, Hu et al. [8] reported a high W_{re} of 61 J/cm^3 in $Pb_{0.96}La_{0.04}Zr_{0.98}Ti_{0.02}O_3$ film, but the η of the film was just 33% at 4.3 MV/cm. On the contrary, Kang et al. [9] reported a relatively higher η (78.9%) of PLZST film, but the W_{re} of the film was just 13 J/cm^3.

The recoverable energy storage density of AFE materials can be calculated by $W_{re} = \int_{P_r}^{P_{max}} EdP$ (E = applied electric field and P = polarization). As shown in Fig. 1, W_{re} is released when the electric field reduces from E_{max} to zero, represented by the green area (W_1, caused by the linear dielectric response) and the yellow area (W_2, caused by the phase transition between FE and AFE phase after electric field removal). The electric energy loss density W_{loss} is represented by the red area and η is defined by $\eta = W_{re}/(W_{re} + W_{loss})$. High W_{re} and high η can be obtained simultaneously by increasing W_1 and W_2. Many approaches have been used to improve W_{re} and η simultaneously by enlarging W_2, such as enlarging the transition electric field E_{FA} [10–14]. Besides these, enlarging W_1 can also improve W_{re} and η simultaneously, this possibility was not envisaged to now. From Fig. 1 it is also clear that by enhancing the breakdown electric field W_1 can be enlarged. But AFE films are usually deposited on metallic bottom electrode (like Pt) and so the breakdown voltage is low. The main reason is the existence of a dead layer, which possesses a low ε_r, at the interface between the film and the bottom electrode by diffusion. To suppress this effect, many researches have revealed that the use of oxide bottom electrodes [15,16] is a good way.

In this work the ABO_3-type metallic oxide $(La_{0.7}Sr_{0.3})MnO_3$ (LSMO), which possess a good lattice match with $(Pb_{0.97}La_{0.02})$

* Corresponding authors.
E-mail addresses: chenying@mail.sic.ac.cn (Y. Chen), xldong@mail.sic.ac.cn (X. Dong).

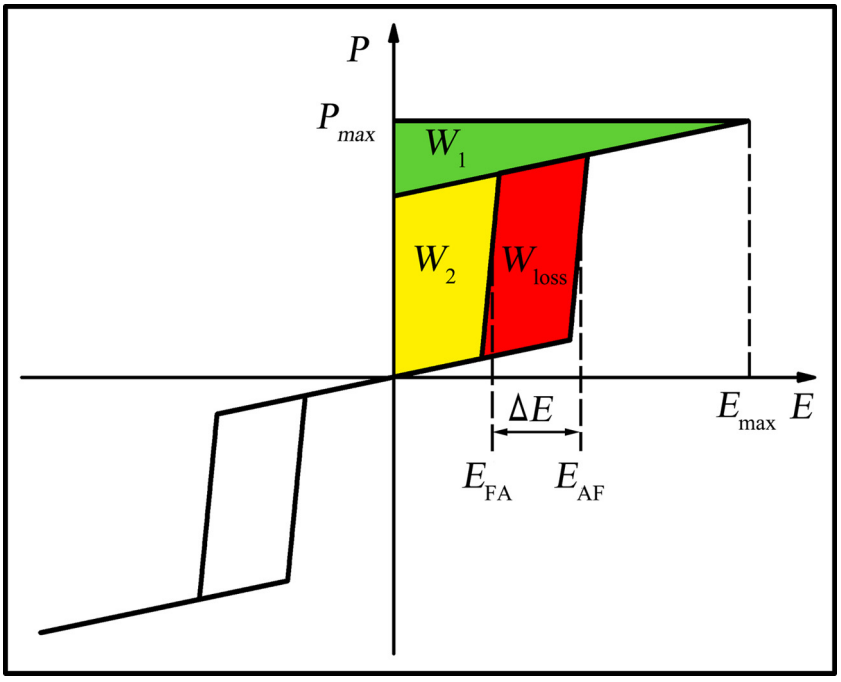

Fig. 1. Schematic diagram of energy storage for antiferroelectric materials.

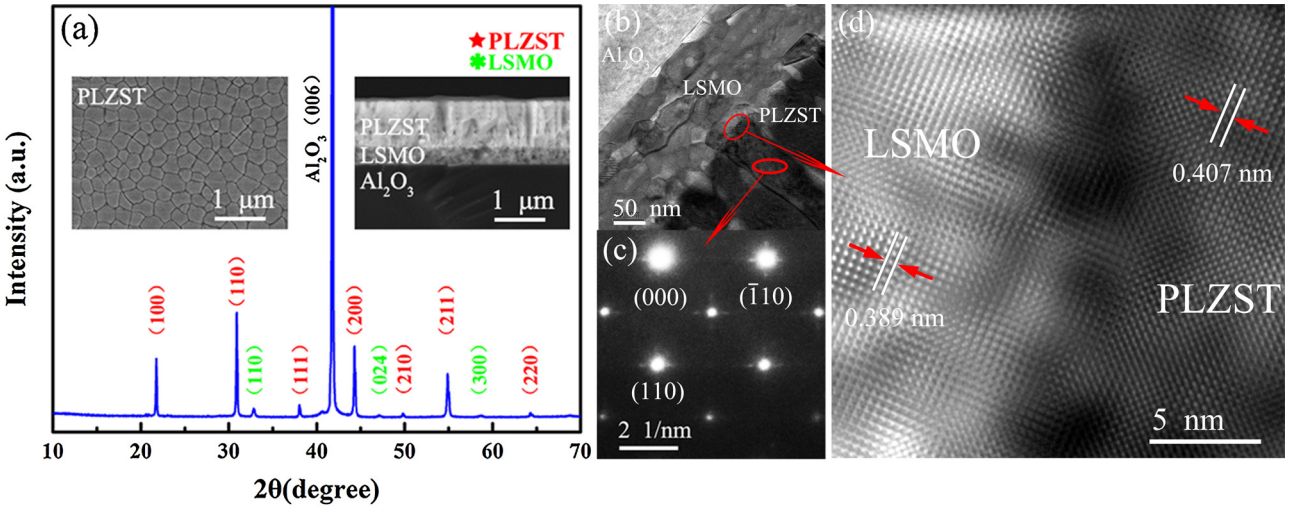

Fig. 2. (a) X-ray diffraction pattern, (inset) surface and cross-section SEM images (b) TEM image of PLZST thin-film deposited on LSMO/Al_2O_3 substrate. (c) Electron diffraction pattern of PLZST thin-film. (d) IFFT image of PLZST/LSMO interface transformed from the high resolution TEM image.

$(Zr_{0.66}Sn_{0.23}Ti_{0.11})O_3$ (PLZST) [12], has been used as a bottom electrode. PLZST thin film was successfully fabricated on LSMO/Al_2O_3(0001) substrate via a chemical solution method. And in our work, we demonstrate that through tuning the interface quality between the film and the substrate and taking full advantage of the linear response after the AFE-FE phase transition, both high energy storage density and high efficiency of AFE materials can be achieved.

2. Experimental procedure

Both the $(Pb_{0.97}La_{0.02})(Zr_{0.66}Sn_{0.23}Ti_{0.11})O_3$ thin-film and $(La_{0.7}Sr_{0.3})MnO_3$ bottom electrode were prepared via chemical solution deposition methods. The detailed deposition process of LSMO can be found elsewhere [17]. The PLZST precursor solution was prepared by dissolving stoichiometric amounts of lead acetate trihydrate, lanthanum acetate, zirconium propoxide, tin acetate and titanium isopropoxide into glacial acetic acid and deionized water co-solvents. Lactic acid (HL) functioned as catalyzer and chelation was added into the solution with mole ratio of Pb:HL = 1:1. Ethylene glycol (EG) was added into the solution with mole ratio of Pb:EG = 1:1 to improve the mechanical properties of the gel. 20 mol% excess lead acetate trihydrate was added into the solution to compensate the lead loss. Each PLZST layer was firstly spin-coated at 5000 rpm for 30 s. Then the wet films were dried at 350 °C and pyrolyzed at 600 °C. This process was repeated several times to achieve the desired thickness. A PbO capping layer was deposited prior to the final annealing at 700 °C to prevent lead loss and to form pure perovskite phase. Finally, gold pads of 0.25 mm in diameter were coated on the film surface as top electrodes by DC sputtering to fabricate capacitors.

The crystallinity was analyzed by X-ray diffraction (XRD, D/MAX-2550V; Rigaku, Tokyo, Japan). Surface and cross-section morphologies were characterized by scanning electron microscope (SEM, S4800; Hitachi, Tokyo, Japan). TEM studies were performed using a Cs-corrected STEM (JEM-2100F, JEOL, Co., Tokyo, Japan). The temperature

dependence of electric constant (ε_r) was measured by a Hewlett Packard LCR meter (1-2-3, Murotanim Nishi-ku, Kobe-shi, Hyogo, 651-22 Japan). The polarization-electric field (*P-E*) loops were characterized by Aix ACCT Co., Azchen, Germany) at 100 Hz.

3. Results and discussion

Fig. 2(a) gives the indexed XRD pattern of PLZST thin-film deposited on LSMO/Al_2O_3(0001) substrate. The PLZST thin-film features a pure perovskite phase with a pseudocubic structure due to the applying of PbO capping layer [18]. The XRD pattern also reveals that the thin-film is polycrystalline and randomly oriented. The SEM images inset in Fig. 2(a) displays that the PLZST thin-film possesses a dense and uniform microstructure with no micro crack. Moreover the PLZST thin-film presents a column-like structure due to heterogeneous nucleation growth [19], and the film thickness is approximately 650 nm. Fig. 2(b) shows the TEM image of PLZST thin-film, the satellite spots in Fig. 2(c) reveal a typical antiferroelectric nature of PLZST thin-film [20]. Fig. 2(d) is the inverse fast Fourier transform (IFFT) image of the LSMO/PLZST interface, which is transformed from the high resolution TEM image. In Fig. 2(d). It is obviously seen that the distance between neighboring (001) planes in both LSMO (0.389 nm) and PLZST (0.407 nm) layers are quite close to each other and the lattice distributions of LSMO and PLZST are transited smoothly through the interface, which shows a good lattice match between LSMO and PLZST. The good lattice match will definitely play an import role in the electrical properties of the PLZST films by reducing the dead layer effect [21].

The temperature dependent dielectric constant (ε_r–*T*) and its reciprocal ($1/\varepsilon_r$–*T*) of PLZST thin-film are plotted in Fig. 3. The linear decrease of $1/\varepsilon_r$ indicates that no phase transition happens during the heating process from 300 K to 400 K [22]. Moreover the low dielectric loss of PLZST thin-film, which changes from 0.015 to 0.030 during the heating process at 100 Hz, confirms the high quality of the LSMO/PLZST interface and will play an important role in improving η.

Fig. 4(a) presents a bipolar *P-E* hysteresis loop of the PLZST thin-film measured at 260 kV/cm. The double loops and the nearly zero remnant polarization demonstrates a typical very fine antiferroelectric nature of PLZST thin-film. The maximum polarization (P_{max}) of PLZST thin-film at 260 kV/cm is 37 μC/cm^2. The backward threshold field (E_{FA}) for phase switching between FE and AFE states is 72 kV/cm. Fig. 4(b) presents the unipolar *P-E* hysteresis loops of PLZST thin-film under various electric fields. The PLZST thin-film shows excellent electric field endurance. The P_{max} of the film is 65.9 μC/cm^2 under a high electric field of 4 MV/cm. Many researches have demonstrated that using ABO_3-type oxide electrodes instead of metallic electrodes will introduce an ion interdiffusion layer along the interface which originates from the ions substituting at the A- or B-sites. This ion interdiffusion layer with continuous distribution of ε_r can smooth the distribution of interfacial electric field [15]. The good lattice match between LSMO and PLZST and very similar thermal expansivity between Al_2O_3 and PLZST [23] also play a key role on this behavior.

We have calculated W_{re} and η as a function of the electric field and the results are presented in Fig. 4(c). We can observe a sharp increase of W_{re} at low electric fields, which is consistent with the phase transition between AFE and FE phases. Meanwhile η shows a sharp decrease at the same electric field which reveals that the increasing of $\triangle E$ can extremely reduce the value of η. The lowest point of η is achieved at an electric field of 260 kV/cm followed by a rapid increase until reaching the maximum of polarization. At 2.2 MV/cm η reaches its maximum value (88.4%) and W_{re} is equal to 23.6 J/cm^3. Finally at 4 MV/cm, W_{re} reaches its maximal value (46.3 J/cm^3) with η always at a high value (84%). The high values of W_{re} and η originate from the high W_1. These results revealed that W_1 played a significant role in the energy storage performance. The results were also compared with other reports summarized from previous literatures [9–14,24–34], as shown in Fig. 4(d). It can be seen that our PLZST thin film properties are among the highest level when W_{re} and η are considered simultaneously. For future applications these two parameters are necessary to favor.

In the same way, temperature stability and fatigue endurance are also two important factors that must be considered in commercialized applications. So these two properties were also evaluated in this work. Fig. 5(a) presents the unipolar *P-E* hysteresis loops of PLZST thin-film under an electric field of 2.2 MV/cm at various temperatures and the inset of Fig. 5(a) is the temperature-dependence of W_{re} and η. The PLZST thin-film shows an excellent thermal stability. With increasing temperature from 300 K to 380 K, the reduction of W_{re} is just 1.3% and η keeps above 70% during the heating process. These results are in perfect agreement with the above-discussed conclusions extracted from Fig. 3 which should be ascribed to the steady AFE state of PLZST with

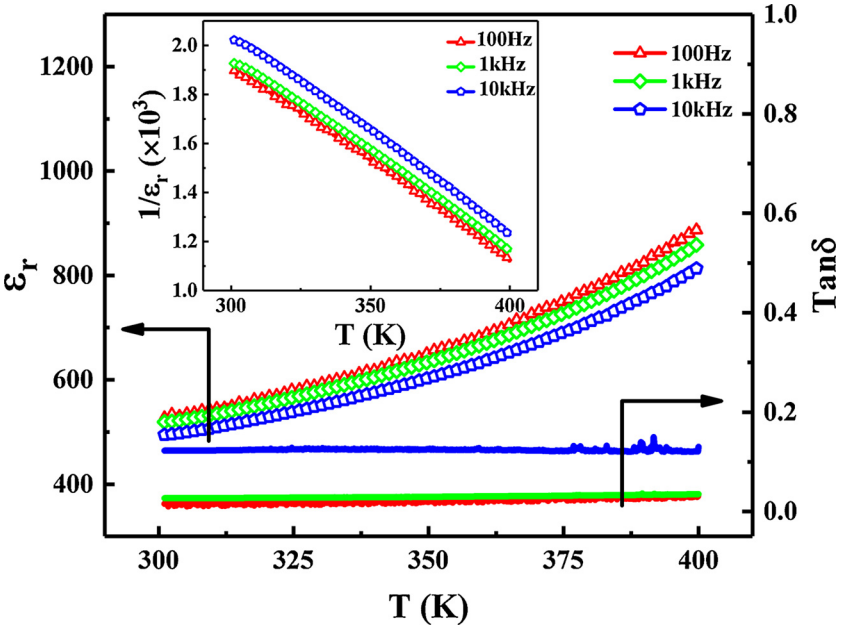

Fig. 3. Temperature dependence of dielectric constant and loss of PLZST thin-film at different frequencies. The inset is the temperature dependence reciprocal dielectric constant of PLZST thin-film at different frequencies.

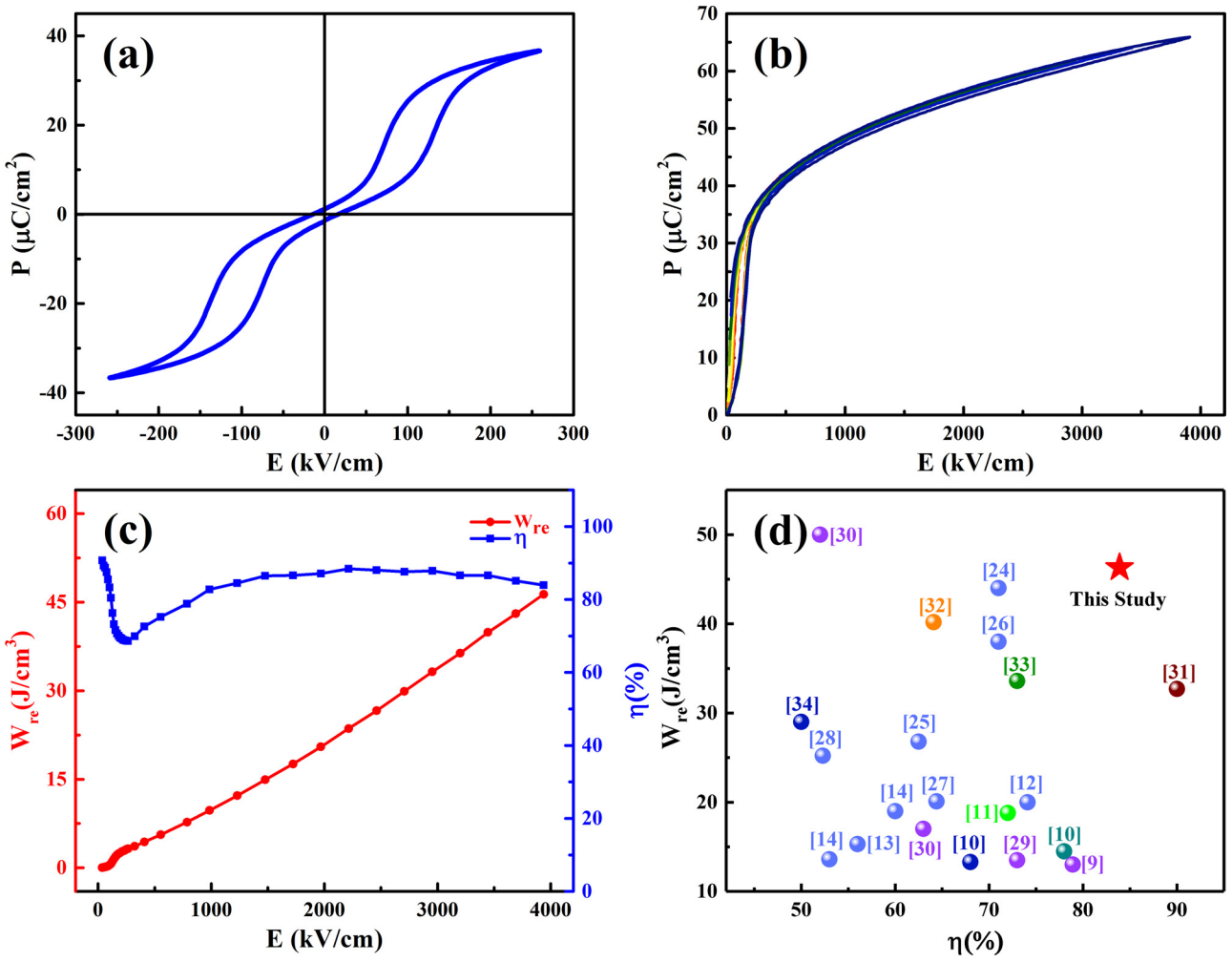

Fig. 4. (a) *P-E* hysteresis loop of the PLZST thin-film at a low electric field. (b) *P-E* hysteresis loops of the PLZST thin film under various electric fields (c) W_{re} and η of PLZST thin film under various electric fields. (d) A summary of energy density data of recently reported antiferroelectric films.

increasing temperature from 300 K to 380 K [35].

Fig. 5(b) presents the unipolar *P-E* hysteresis loops of PLZST thin-film, which is investigated as a function of the charge-discharge cycling up to 1×10^5 cycles. The electric field cycling test was carried out with an electric field of 2.2 MV/cm and a frequency of 1 kHz at room temperature. As the cycling test going on, the *P-E* hysteresis loops keep slim and the P_{max} shows a slightly decreasing tendency. The variations of W_{re} and η during the fatigue test are given in the inset of Fig. 5(b). After

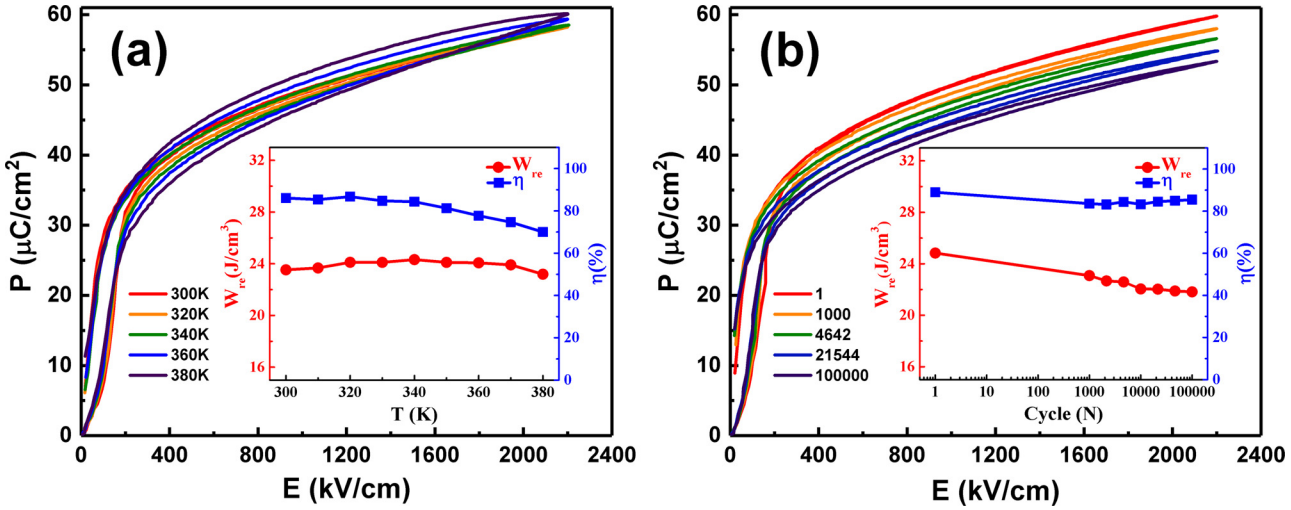

Fig. 5. (a) Temperature and (b) fatigue dependence of*P-E* hysteresis loops, W_{re} and η of PLZST thin-film. The tests were performed under an electric field of 2.2 MV/cm.

1×10^5 charge-discharge cycles W_{re} changes from 25 J/cm^3 to 22 J/cm^3 and the η kept above 83%. These excellent performances are closely linked to the use of oxide as electrodes. Firstly, oxide electrodes can reduce the dead layer effect by establishing a strong adhesion layer at the interface and providing a sink for oxygen vacancies [16,36,37]. Secondly, the using of Al_2O_3 and LSMO in this work can further reduce the dead layer effect because of less thermal and lattice mismatch.

4. Conclusions

In summary, a high quality PLZST thin film was fabricated on LSMO/Al_2O_3(0001) substrate by a modified sol-gel method. A high energy storage density of 46.3 J/cm^3 together with a high energy storage efficiency of 84% was obtained at room temperature, benefiting mainly from the linear dielectric response and the use of oxide electrodes. Moreover the thin-film also exhibited excellent temperature stability and high fatigue endurance. The recoverable energy storage density decreased from 23.5 to 23.2 J/cm^3 with increasing temperature from 300 K to 380 K and was able to withstand fatigue endurance up to 1×10^5 cycling. These excellent properties indicate the PLZST thin film obtained here can have promising potential in high energy storage capacitors.

Acknowledgements

This work was supported by the National Natural Science Foundation of China (Nos. U1530156 and 11774366), International Partnership Program of Chinese Academy of Sciences (Grant No. GJHZ1821), Chinese Academy of Sciences President's International Fellowship Initiative (Grant No. 2017VEA0002), and Shanghai Sailing Program (No. 17YF1429700).

References

[1] Z. Yao, Z. Song, H. Hao, Z. Yu, M. Cao, S. Zhang, M.T. Lanagan, H. Liu, Homogeneous/inhomogeneous-structured dielectrics and their energy-storage performances, Adv. Mater. 29 (20) (2017) 15.
[2] Z. Liu, Y. Bai, X.F. Chen, X.L. Dong, H.C. Nie, F. Cao, G.S. Wang, Linear composition-dependent phase transition behavior and energy storage performance of tetragonal PLZST antiferroelectric ceramics, J. Alloys Compd. 691 (2017) 721–725.
[3] C.H. Xu, Z. Liu, X.F. Chen, S.G. Yan, F. Cao, X.L. Dong, G.S. Wang, High charge-discharge performance of Pb0.$La_{0.02}(Zr_{0.35}Sn_{0.55}Ti_{0.10})_{0.995}O_3$ antiferroelectric ceramics, J. Appl. Phys. 120 (7) (2016) 6.
[4] X.H. Hao, J.W. Zhai, L.B. Kong, Z.K. Xu, A comprehensive review on the progress of lead zirconate-based antiferroelectric materials, Prog. Mater. Sci 63 (2014) 1–57.
[5] X. Wang, T. Yang, J. Shen, D. Damjanovic, High-energy storage performance in $(Pb0.La_{0.02})(Zr_{0.45}Sn_{0.55})_{0.995}O_3$ AFE thick films fabricated via a rolling process, J. Am. Ceram. Soc. 99 (11) (2016) 3569–3572.
[6] L. Zhang, S. Jiang, B. Fan, G. Zhang, High energy storage performance in $(Pb0.Ba_{0.1}La_{0.02}Y_{0.008})(Zr_{0.65}Sn_{0.3}Ti_{0.05})O_3$- $(Pb_{0.97}La_{0.02})(Zr_{0.9}Sn_{0.05}Ti_{0.05})O_3$ antiferroelectric composite ceramics, Ceram. Int. 41 (1) (2015) 1139–1144.
[7] R. Xu, B. Li, J. Tian, Z. Xu, Y. Feng, X. Wei, D. Huang, L. Yang, $Pb_{0.94}La_{0.04}[(Zr_{0.70}Sn_{0.30})_{0.90}Ti_{0.10}]O_3$ antiferroelectric bulk ceramics for pulsed capacitors with high energy and power density, Appl. Phys. Lett. 110 (14) (2017) 142904.
[8] Z.Q. Hu, B.H. Ma, R.E. Koritala, U. Balachandran, Temperature-dependent energy storage properties of antiferroelectric $Pb0.La_{0.04}Zr_{0.98}Ti_{0.02}O_3$ thin films, Appl. Phys. Lett. 104 (26) (2014) 263902.
[9] S.B. Kang, M.G. Choi, D.Y. Jeong, Y.M. Kong, J. Ryu, Energy storage properties of nano-grained antiferroelectric $(Pb,La)(Zr,Ti)O_3$ films prepared by aerosol-deposition method, IEEE Trans. Dielectr. Electr. Insul. 22 (3) (2015) 1477–1482.
[10] X.H. Hao, J.W. Zhai, X. Yao, Improved energy storage performance and fatigue endurance of sr-doped $PbZrO_3$ antiferroelectric thin films, J. Am. Ceram. Soc. 92 (5) (2009) 1133–1135.
[11] M. Ye, Q. Sun, X.Q. Chen, Z.H. Jiang, F.P. Wang, Effect of Eu doping on the electrical properties and energy storage performance of $PbZrO_3$ antiferroelectric thin films, J. Am. Ceram. Soc. 94 (10) (2011) 3234–3236.
[12] H. Pan, Y. Zeng, Y. Shen, Y.H. Lin, C.W. Nan, Thickness-dependent dielectric and energy storage properties of $(Pb0.La_{0.04})(Zr_{0.98}Ti_{0.02})O_3$ antiferroelectric thin films, J. Appl. Phys. 119 (12) (2016) 5.
[13] X.G. Fang, S.X. Lin, A.H. Zhang, X.B. Lu, X.S. Gao, M. Zeng, J.M. Liu, Effect of bottom electrodes on polarization switching and energy storage properties in $Pb0.La_{0.02}(Zr_{0.95}Ti_{0.05})O_3$ antiferroelectric thin films, Solid State Commun. 219 (2015) 39–42.
[14] J. Ge, X.L. Dong, Y. Chen, F. Cao, G.S. Wang, Enhanced polarization switching and energy storage properties of $Pb0.La_{0.02}(Zr_{0.95}Ti_{0.05})O_3$ antiferroelectric thin films with $LaNiO_3$ oxide top electrodes, Appl. Phys. Lett. 102 (14) (2013) 4.
[15] C. Hou, W. Huang, W. Zhao, D. Zhang, Y. Yin, X. Li, Ultrahigh energy density in $SrTiO_3$ film capacitors, ACS Appl. Mater. Interfaces 9 (24) (2017) 20484–20490.
[16] Q. Yang, J.X. Cao, Y.C. Zhou, L.Z. Sun, X.J. Lou, Dead layer effect and its elimination in ferroelectric thin film with oxide electrodes, Acta Mater. 112 (2016) 216–223.
[17] B. Zhao, Y. Chen, F. Xue, X. Guo, G.S. Wang, L.H. Yang, W.S. Wang, X.L. Dong, Magnetic and electric properties of wrinkled manganite films derived by sol-gel method, J. Am. Ceram. Soc. 100 (6) (2017) 2392–2396.
[18] M.S. Mirshekarloo, K. Yao, T. Sritharan, Large strain and high energy storage density in orthorhombic perovskite, $(Pb0.La_{0.02})(Zr_{1-x-y}Sn_xTi_y)O_3$ antiferroelectric thin films, Appl. Phys. Lett. 97 (14) (2010) 142902.
[19] P.M. Leufke, R. Kruk, R.A. Brand, H. Hahn, In situ magnetometry studies of magnetoelectric LSMO/PZT heterostructures, Phys. Rev. B 87 (9) (2013) 9.
[20] H. He, X. Tan, Electric-field-induced transformation of incommensurate modulations in antiferroelectric $Pb0.Nb_{0.02}[(Zr_{1-x}Sn_x)_{1-y}Ti_y]_{0.98}O_3$, Phys. Rev. B 72 (2) (2005) 024102.
[21] A. Lubk, M.D. Rossell, J. Seidel, Y.H. Chu, R. Ramesh, M.J. Hytch, E. Snoeck, Electromechanical coupling among edge dislocations, domain walls, and nanodomains in $BiFeO_3$ revealed by unit-cell-wise strain and polarization maps, Nano Lett. 13 (4) (2013) 1410–1415.
[22] Z. Liu, X. Chen, W. Peng, C. Xu, X. Dong, F. Cao, G. Wang, Temperature-dependent stability of energy storage properties of $Pb0.La_{0.02}(Zr_{0.58}Sn_{0.335}Ti_{0.085})O_3$ antiferroelectric ceramics for pulse power capacitors, Appl. Phys. Lett. 106 (26) (2015) 262901.
[23] G. Shirane, K. Suzuki, A. Takeda, Phase transitions in solid solutions of $PbZrO_3$ and $PbTiO_3$ (II) X-Ray study, J. Phys. Soc. Jpn. 7 (1) (1952) 12–18.
[24] Y. Zhao, X.H. Hao, Q. Zhang, Enhanced energy-storage performance and electrocaloric effect in compositionally graded $Pb(1-3x/2)La_xZr_{0.85}Ti_{0.15}O_3$ antiferroelectric thick films, Ceram. Int. 42 (1) (2016) 1679–1687.
[25] C. Liu, S.X. Lin, M.H. Qin, X.B. Lu, X.S. Gao, M. Zeng, Q.L. Li, J.M. Liu, Energy storage and polarization switching kinetics of (001)-oriented $Pb0.La_{0.02}(Zr_{0.95}Ti_{0.05})O_3$ antiferroelectric thick films, Appl. Phys. Lett. 108 (11) (2016) 5.
[26] Y. Zhao, X. Hao, Q. Zhang, Energy-storage properties and electrocaloric effect of $Pb(1-3x/2)La_xZr_{0.85}Ti_{0.15}O_3$ antiferroelectric thick films, ACS Appl. Mater. Interfaces 6 (14) (2014) 11633–11639.
[27] Y.Y. Liu, Y. Wang, X.H. Hao, J.B. Xu, Preparation and energy-storage performance of PLZT antiferroelectric thick films via sol-gel method, Ceram. Int. 39 (2013) S513–S516.
[28] Y. Wang, X.H. Hao, J.B. Xu, Effects of PbO insert layer on the microstructure and energy storage performance of (042)-preferred PLZT antiferroelectric thick films, J. Mater. Res. 27 (13) (2012) 1770–1775.
[29] Y. Zhao, H.C. Gao, X.H. Hao, Q. Zhang, Orientation-dependent energy-storage performance and electrocaloric effect in PLZST antiferroelectric thick films, Mater. Res. Bull. 84 (2016) 177–184.
[30] X.H. Hao, Y. Wang, L. Zhang, L.W. Zhang, S.L. An, Composition-dependent dielectric and energy-storage properties of $(Pb,La)(Zr,Sn,Ti)O_3$ antiferroelectric thick films, Appl. Phys. Lett. 102 (16) (2013) 4.
[31] C.W. Ahn, G. Amarsanaa, S.S. Won, S.A. Chae, D.S. Lee, I.W. Kim, Antiferroelectric thin-film capacitors with high energy-storage densities, low energy losses, and fast discharge times, ACS Appl. Mater. Interfaces 7 (48) (2015) 26381–26386.
[32] B. Peng, Q. Zhang, X. Li, T. Sun, H. Fan, S. Ke, M. Ye, Y. Wang, W. Lu, H. Niu, X. Zeng, H. Huang, Large energy storage density and high thermal stability in a highly textured (111)-oriented $Pb_{0.8}Ba_{0.2}ZrO_3$ relaxor thin film with the coexistence of antiferroelectric and ferroelectric phases, ACS Appl. Mater. Interfaces 7 (24) (2015) 13512–13517.
[33] H.C. Gao, X.H. Hao, Q.W. Zhang, S.L. An, L.B. Kong, Electrocaloric effect and energy-storage performance in grain-size-engineered PBLZT antiferroelectric thick films, J. Mater. Sci.-Mater. Electron. 27 (10) (2016) 10309–10319.
[34] M.H. Park, H.J. Kim, Y.J. Kim, T. Moon, K.D. Kim, C.S. Hwang, Thin $Hf_xZr_{1-x}O_2$ films: a new lead-free system for electrostatic supercapacitors with large energy storage density and robust thermal stability, Adv. Energy Mater. 4 (16) (2014) 1400610.
[35] Z. Liu, X.L. Dong, Y. Liu, F. Cao, G.S. Wang, Electric field tunable thermal stability of energy storage properties of PLZST antiferroelectric ceramics, J. Am. Ceram. Soc. 100 (6) (2017) 2382–2386.
[36] M.D. Nguyen, C.T.Q. Nguyen, H.N. Vu, G. Rijnders, Controlling microstructure and film growth of relaxor-ferroelectric thin films for high break-down strength and energy-storage performance, J. Eur. Ceram. Soc. 38 (1) (2018) 95–103.
[37] X.J. Lou, J. Wang, Unipolar and bipolar fatigue in antiferroelectric lead zirconate thin films and evidences for switching-induced charge injection inducing fatigue, Appl. Phys. Lett. 96 (10) (2010) 102906.